RESEARCH ARTICLE
ATMOSPHERIC PHYSICS

Earth and Planetary Physics
10: 167–175, 2026
doi: 10.26464/epp2026009

Stratospheric transport and residence time of Hunga volcanic aerosol

Qing Zhao, and Xin Zhou*

School of Atmospheric Sciences, Chengdu University of Information Technology, Chengdu 610225, China

Key Points:

- Hunga volcanic water vapor accelerated sulfate aerosol growth but shortened the stratospheric lifetime to 14 months by enhancing gravitational settling.
- Volcanic aerosols reached the polar vortices months after water vapor despite similar global diffusion patterns.
- The extreme injection altitude prolonged aerosol residence; however, high water vapor appears to have had an effect on the aerosol lifetime.

Citation: Zhao, Q., and Zhou, X. (2026). Stratospheric transport and residence time of Hunga volcanic aerosol. *Earth Planet. Phys.*, *10*(1), 167–175. http://doi.org/10.26464/epp2026009

Abstract: The January 2022 eruption of Hunga injected unprecedented volumes of water vapor (150 Tg) and modest sulfur dioxide (SO_2) into the stratosphere, producing accelerated sulfate aerosol formation in the early plume. As the aerosols gradually spread into the global stratosphere, the role of water vapor, among other factors in the spread and residence time of the sulfate aerosols, remained unclear. We used multisatellite observations to better understand the role of water vapor in the spread and lifetime of Hunga volcanic aerosols. Stratospheric circulation transported the plumes to ~26 km within the polar vortices—the Antarctic by August 2022 and the Arctic by January 2023—with the arrival of aerosols lagging behind that of water vapor by months. Even though high injection altitudes (58 km) and strong Brewer–Dobson circulation contributed to prolonging the residence time of aerosols, the water vapor enhanced particle growth and thus accelerated gravitational settling, with the half lifetime of aerosols being 14 months. Our analysis revealed a critical trade-off: after the eruption of the Hunga volcano, an extremely high injection height and strong upward motion slowed the removal of aerosols, but extreme water vapor loading still had a certain impact on the half lifetime of the aerosols. These findings highlight the role of water vapor in the persistence of aerosols from submarine eruptions.

Keywords: stratosphere; water vapor; aerosol lifetime; volcanic activity

1. Introduction

The violent eruption of the Hunga volcano (20.54°S, 175.38°W), which commenced on January 14, 2022, represents the most explosive event in the modern observational era, with an estimated Volcanic Explosivity Index of 5.81 (Khaykin et al., 2022). The massive eruption persisted over several days, with a particularly intense phase occurring on January 15, 2022, amplified by magma–water interaction. This interaction generated a volcanic plume reaching an unprecedented height of 57 km, which penetrated directly through the stratosphere into the mesosphere (Carr et al., 2022; Proud et al., 2022; Taha et al., 2022). Enhanced aerosol extinction above 45 km was subsequently detected by the Ozone Mapping and Profiler Suite Limb Profiler (OMPS-LP; Schoeberl et al., 2022; Taha et al., 2022).

Of particular significance was the unprecedented injection of water vapor (H_2O) into the atmosphere by this eruption, setting records in both injection altitude and total stratospheric H_2O mass since Microwave Limb Sounder (MLS) observations began. The direct H_2O injection was estimated at approximately 146 ± 5 Tg, increasing the global stratospheric water vapor (SWV) burden by approximately 10% (Khaykin et al., 2022; Millán et al., 2022; Xu JY et al., 2022). In contrast, the total sulfur dioxide (SO_2) emission was moderate, estimated at only 0.5 Tg (Millán et al., 2022). The abundance of H_2O facilitated the rapid conversion of erupted SO_2 into sulfate aerosols (Legras et al., 2022; Zhu YQ et al., 2022). The direct injection of massive amounts of H_2O into the stratosphere by this eruption initially caused stratospheric cooling (Schoeberl et al., 2022). However, 2 weeks posteruption, radiative heating from the H_2O began to dominate the top-of-atmosphere radiative forcing owing to dispersion and dilution, which was proposed to result in a net warming of the climate system (Jenkins et al., 2023; Sellitto et al., 2022). Recent studies suggested that excess water vapor from Hunga cooled, instead of warmed, the Southern Hemisphere in the 2 years posteruption, after considering the cooling effect of sulfate aerosols and Hunga-induced ozone loss (Gupta et al., 2025; Stenchikov et al., 2025). Apart from the radiative impacts, the

First author: Q. Zhao, zhaoq2021013307@163.com
Correspondence to: X. Zhou, Zhouxin18@cuit.edu.cn
Received 26 JUN 2025; Accepted 08 SEP 2025.
First Published online 30 SEP 2025.

excess H_2O was observed to cause ozone loss via heterogeneous chlorine activation on humidified volcanic aerosols within just 1 week after the eruption (Evan et al., 2023). Increased OH radicals from H_2O led to global ozone reductions of 2%–10% in the upper stratosphere and mesosphere (Fleming et al., 2024; Zhou X et al., 2024). In the Antarctic region, the excess H_2O contributed to additional chemical ozone depletion (up to 10 Dobson units) via increased heterogeneous chemical processes over the polar stratospheric clouds, with the effect maximized on the vortex edge in the 2023 Antarctic spring season (Zhou X et al., 2024).

The effects of volcanic injections are not instantaneous; they can persist in the stratosphere for several years. The spread and residence time of the Hunga plume is thus important for understanding the impacts of Hunga on climate change and ozone depletion. However, the spread and residence time of volcanic aerosols varies between events because these factors depend on the height and latitude of the injection and the stratospheric circulation patterns (Schoeberl et al., 2025; Toohey et al., 2025). The Hunga eruption, as an exceptional case, simply added more complexity, with humidity arising as an obvious factor. In this work, we investigated the global atmospheric dispersion processes of the aerosol plume following the Hunga Tonga eruption by combining satellite observations with aerosol e-folding model fitting. We further examined factors influencing the aerosol lifetime by using multiple historical volcanic eruptions. This study focuses on the timing of the volcanic plume arrival within the polar vortex and factors controlling the posteruption aerosol lifetime. Our work is broadly relevant to the radiative forcing effects of stratospheric sulfate aerosols, their potential subsequent climate impacts, and their overall integrated effects.

2. Materials and Methods

To quantify the water vapor from volcanic eruption events, we calculated the SWV in the tropics. Data for the El Chichón, Pinatubo, and Hunga eruptions were obtained from previous studies (Walter and de Silva, 1991; Kroll et al., 2021; Xu JY et al., 2022). For the other volcanic events that were chosen for examination, their SWV data were calculated from MLS satellite observations. We averaged the daily water vapor values between 30°N and 30°S latitude after each volcanic eruption and then summed the values across all pressure levels above 100 hPa over a 2-year period to obtain the final measurements. The SO_2 injection height data for each volcanic event were entirely sourced from previous studies (Carey and Sigurdsson, 1986; Holasek et al., 1996; Bourassa et al., 2012; Suzuki and Iguchi, 2019; Klekociuk et al., 2020; Kloss et al., 2021; Zhu YQ et al., 2022; Axebrink et al., 2025). The strength of the Brewer–Dobson vertical velocity component (W^*) was calculated using the ERA5 monthly mean dataset (fifth generation of the European Centre for Medium-Range Weather Forecasts's atmospheric reanalysis dataset; Hersbach et al., 2020) of pressure levels from 1940 to the present, which includes reanalysis data on meridional wind, vertical velocity, and temperature.

The Brewer–Dobson circulation is a large-scale meridional circulation in the stratosphere characterized by ascent in the tropics and descent in the polar regions. Its vertical velocity component (W^*) is primarily driven by the residual circulation induced by planetary wave breaking. Component W^* fundamentally represents the theoretical expression of the vertical velocity in the Brewer–Dobson circulation under the transformed Eulerian mean framework, reflecting the modification of the mean vertical circulation by eddy fluxes (e.g., planetary waves). In this study, the calculation of W^* was initiated by computing the zonal-mean vertical velocity, expressed by the following formulas, where W^* is the raw vertical velocity (in pascals per second) and λ denotes longitude. Subsequently, W^* was calculated through the fundamental equation of transformed Eulerian mean theory:

$$\overline{w} = \frac{1}{2\pi}\int_0^{2\pi} w\mathrm{d}\lambda, \tag{1}$$

$$W^* = \overline{w} + \frac{1}{a\cos\varphi} g \cdot \frac{\partial}{\partial\varphi}(\overline{v'\theta'}\cos\varphi). \tag{2}$$

This value was then unit-converted to millimeters per second, yielding the final residual vertical velocity W^*:

$$W^* = -\frac{H}{p} g w, \tag{3}$$

Where W^* is in mm/s, $H = 7000$ m.

The fitting of the aerosol half lifetime was based on an exponential decay model. This model is commonly utilized to describe the natural attenuation processes of substances over time. In this study, it was used to simulate the time-dependent variation of aerosol optical depth (AOD). When calculating the half lifetime, we first used the month before the volcanic eruption as a reference to calculate the time series of AOD anomalies after each volcanic eruption. We determined the time when the AOD anomaly reached its peak, which was the lag time, and then began the half lifetime fitting from that month, following Toohey et al. (2025). Finally, with the month of the volcanic eruption as Month 0, we calculated the time it took for the AOD value to drop to half of the AOD anomaly value corresponding to the lag time, based on both the AOD anomaly time series and the half lifetime curve fitted by the exponential model, thereby obtaining two corresponding decay times.

3. Data

Satellite observation data of water vapor were obtained from the MLS on board the Aura Satellite (Waters et al., 2006). The data version was 4.2. The satellite data consisted of daily gridded water vapor observations along the 180° longitude from January 1, 2004, to December 26, 2023. The water vapor data for each grid point included 64 latitudes, ranging from 87.8°S to 87.8°N, and 47 pressure levels, ranging from 1000 to 0.1 hPa.

The data on sulfate aerosols were obtained from the OMPS-LP on board the Suomi-NPP satellite and Global Space-based Stratospheric Aerosol Climatology (GloSSAC) satellite observation data. These data comprise a 44-year climatology of stratospheric aerosol properties focused on extinction coefficient measurements. We used the daily mean AOD measurements at 510 nm, a key parameter quantifying the total extinction of solar radiation by aerosol particles within a vertical column of the atmosphere, from the version 2.1 of OMPS-LP satellite data (Taha et al., 2021) from January 1, 2022, to June 18, 2024, and along the 180° longitude, and the latitude range covers 36 latitudes from 87.5°S to

87.5°N at 5° intervals. The GloSSAC version 2.22 dataset (NASA/LARC/SD/ASDC, 2024), a global stratospheric aerosol climatology dataset, was used to analyze monthly AOD data at 525 nm across all latitudes from 1979 to 2023.

The water vapor anomalies were obtained by removing the climatology from January 2004 to December 2021. Because this study focuses on the upper troposphere and stratosphere, data from six pressure levels (10–100 hPa) in the month of each volcanic eruption were selected, covering all longitudes (for zonal averaging) and five latitudes (2.5° north and south of the volcanic location).

4. Results

We first show the timing of the volcanic water vapor and aerosols arriving at the polar vortex, which can subsequently destroy ozone. Next, we compare the transport rate of volcanic aerosols in the cases of Hunga and Pinatubo, with the two standing for a water-rich plume and the conventional explosive SO_2 plume, respectively. We then provide the observed residence time of the Hunga volcanic aerosols, in comparison with other historical volcanic events in the satellite era, and explore its dependence on the Brewer–Dobson circulation strength, the altitude of the aerosol injection, and the SWV.

4.1 Global Transport and Diffusion Patterns of Water Vapor and Aerosols

4.1.1 Arrival time of water vapor and aerosol plumes at the polar vortices

The effect of water vapor on the volcanic aerosol in the early stage of the plume by acceleration of the SO_2 oxidation into sulfate aerosols, which subsequently doubled the stratospheric AOD (SAOD), has been documented in previous studies (Zhu YQ et al., 2022). The sulfate aerosols were then gradually transported globally with the Brewer–Dobson circulation, together with the water vapor plume. The timing of the arrival of these substances at the polar vortex is crucial. For instance, in the first year after the eruption, the water vapor plume did not arrive at the Antarctic before the polar vortex was formed, so the loss of Antarctic ozone chemistry was avoided in 2022 (Manney et al., 2023). Thus, we first show the timing of the Hunga aerosols, compared with water vapor, arriving at the polar vortex in both hemispheres.

Because of the stable Antarctic polar vortex during winter, anomalies were confined to altitudes above 26 km. By October, these anomalies dissipated and propagated downward. This downward movement is in agreement with the results of Manney et al. (2023). The Brewer–Dobson circulation transported water vapor to high latitudes in the northern hemisphere during January and February 2023 (northern hemisphere winter). Anomalies initially accumulated at 26 km, then rapidly descended in March as spring began.

Figure 1 shows the time series of the SAOD anomalies at 510 nm over the edge of the polar vortex in the northern hemisphere and southern hemisphere, 62.5°N and 62.5°S, respectively. The SAOD at 62.5°S peaked around December 2022 (~360 days posteruption), whereas water vapor reached 60°S by July 2022 and entered the Antarctic polar vortex in August 2022. This observation indicates delayed aerosol arrival compared with water vapor, although following a similar seasonal transport pattern because of

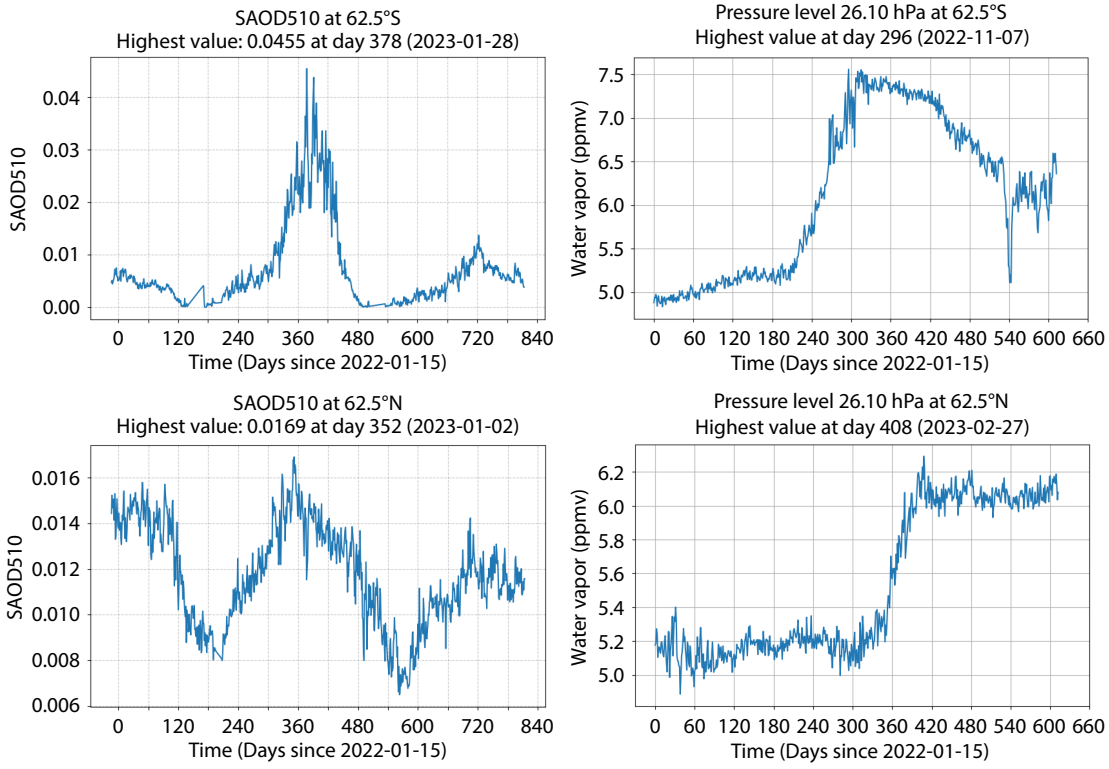

Figure 1. Time series of SAOD anomalies at 510 nm (left panels) and SWV anomalies (right panels; unit: parts per million by volume) at 62.5°S (upper panels) and 62.5°N (lower panels).

the stratospheric circulation. The SAOD at 62.5°N peaked in January 2023 (~352 days posteruption), aligning with the timing of water vapor accumulation in the Arctic upper stratosphere.

Both hemispheres exhibited similar transport mechanisms governed by Brewer–Dobson circulation and seasonal polar vortex dynamics, with water vapor and aerosols first accumulating at specific altitudes before downward movement. The southern hemisphere processes occurred slightly earlier than those in the northern hemisphere because the cross-equator transport was delayed by the westerlies of the Quasi-Biennial Oscillation until its transition to the easterlies.

4.1.2 Comparison of aerosol plume transport between the hunga tonga and pinatubo eruptions

Figure 2a shows distinct differences in the OMPS satellite-derived AOD at 510 nm. After the Hunga eruption, the AOD increased substantially in the 20°N latitude band within 3 months posteruption. By April 2022, the AOD exceeded 0.08 in the 0°–20°S region, peaking at 0.12 near 50°S in July 2022. The AOD signals reached the Antarctic polar vortex ~1 year posteruption and returned to background levels by June 2023 (17 months posteruption). In the case of the 1991 Pinatubo eruption, the AOD peaked in equatorial regions (by 0.18–0.21) 4 months posteruption, followed by poleward diffusion. The Arctic AOD maximum (at 0.21–0.24) occurred 1 year posteruption. Despite differences in the SO_2 and water vapor content, both eruptions exhibited comparable meridional diffusion rates.

The MLS water vapor anomalies (at 26 hPa; Figure 2a) confirmed that water vapor plumes initially followed similar transport pathways as SO_2 plumes but that pronounced water vapor anomalies were observed exclusively in the high northern latitudes, consistent with the exceptionally high water vapor content of Hunga.

4.2 Aerosol Half Lifetime Fitting and Lifetime Analysis

Next, we examined the observed lifetime of Hunga aerosols and analyzed potential drivers by situating the Hunga eruptions within its broader context. Figure 3 shows a time series of AOD and AOD anomalies from 1979 to 2023. Using zonally averaged AOD data (60°N–60°S) from the GloSSAC dataset (525 nm), we defined background AOD levels as the 1997–2005 mean. The AOD anomalies were computed to identify major volcanic events (e.g., the 1982 El Chichón and 1991 Pinatubo eruptions). Post-2006 anomalies (Figure 3c) highlighted smaller scale events, enabling a comparative analysis of aerosol lifetimes. These events are in agreement with previous studies (e.g., Figure 10c in Khaykin et al., 2022).

We separated the changes into lag time and decay time following the method of Toohey et al. (2025). The lag time is the time before the AOD shows signs of decay after injection (see Table 1), whereas the decay time is related to the removal rate and is thus used to calculate the half lifetime.

Figure 4 shows aerosol half lifetime fitting curves for each selected volcanic activity, and Figure 5 shows the normalized plot of the fitted curves for the half lifetimes of volcanic aerosols. An exponential decay model was applied to AOD anomalies from selected eruptions. We first examined the water vapor effects. One would expect that an enhanced water vapor plume would accelerate the removal of aerosols by hygroscopic growth (enhancing dry–wet deposition). In our observations, high water vapor loads (e.g., Hunga with a 14-month half lifetime) shortened lifetimes but were partially offset by the injection height and Brewer–Dobson circulation (W^*).

Table 1 and Figure 6 highlight the relationships between volcanic parameters and aerosol lifetimes. First, higher SO_2 injection heights correlate with longer half lifetimes. For example, El Chichón and Pinatubo demonstrated injection heights leading to 24-month half lifetimes due to bypassing tropospheric scavenging.

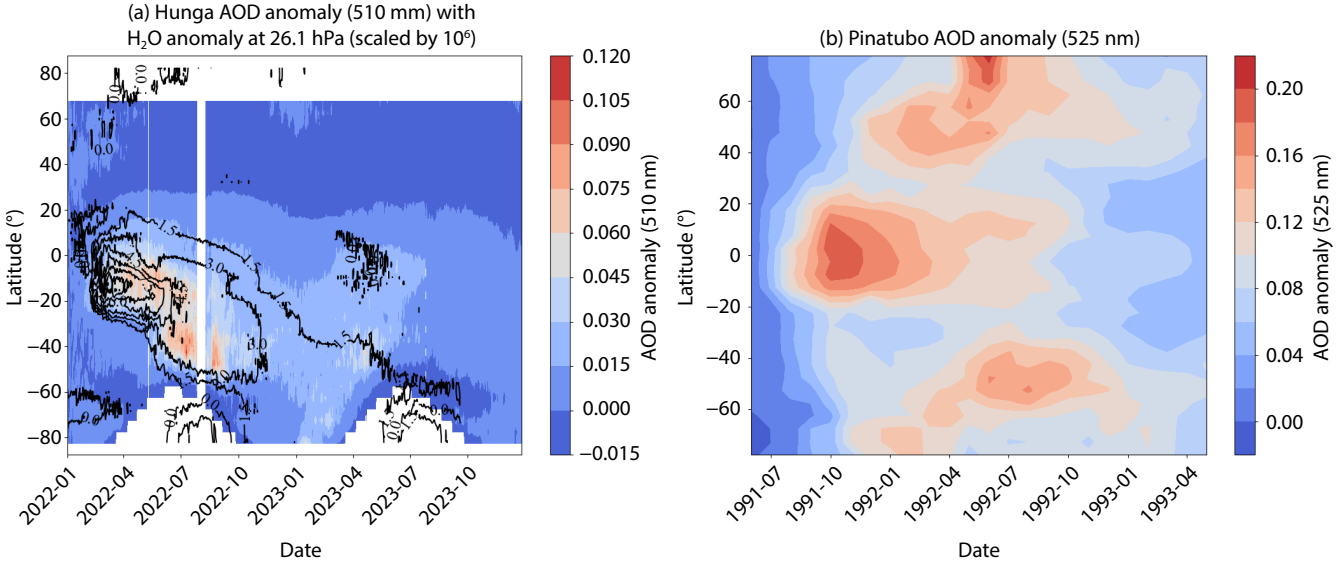

Figure 2. Latitude–time cross sections of the AOD anomalies after the (a) Hunga and (b) Pinatubo eruptions. The black contour lines represent water vapor anomalies after removing the climatology.

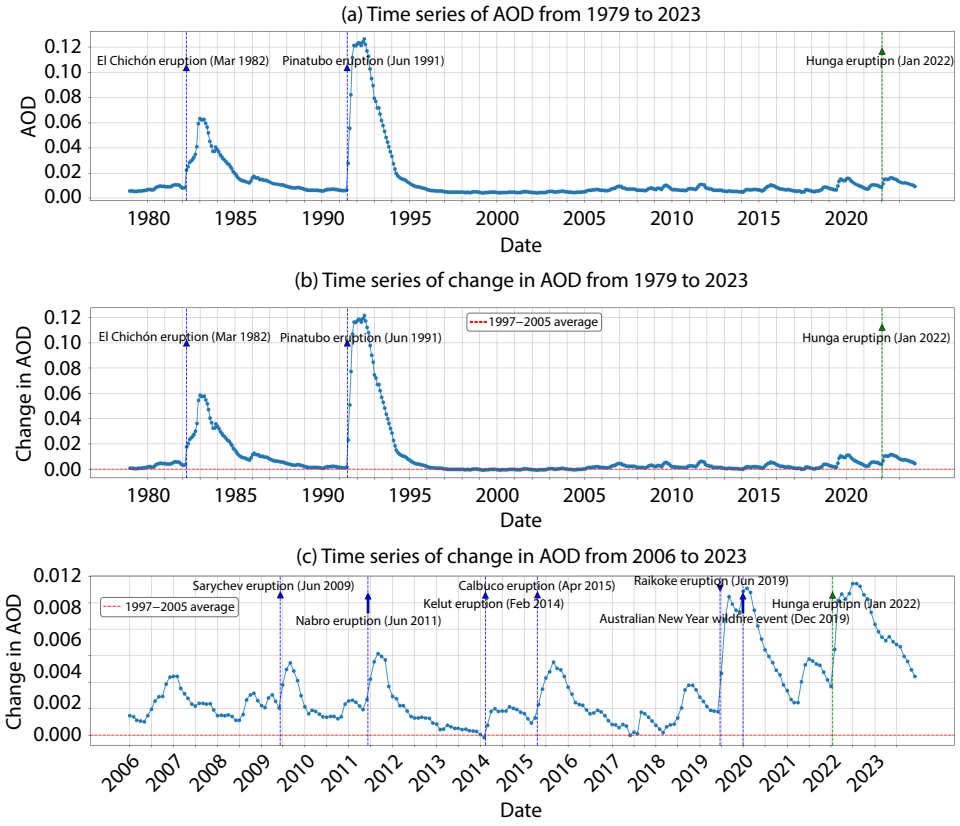

Figure 3. Time series of AOD and AOD anomalies from 1979 to 2023, with large-scale volcanic activities selected and annotated in the figure.

Table 1. Basic information, including comparisons of lag time (months), aerosol half lifetime (months), SWV (ppmv), SO_2 injection height (km), W^* (mm/s), and latitude, of the Hunga eruption and other historical volcanic eruptions.

Volcano	Lag time	Half lifetime	SWV	SO_2	W^*	Latitude	References
El Chichón	10	24	20	29–32	0.489	17.4°N	Carey and Sigurdsson, 1986; Walter and Desilva, 1991
Pinatubo	12	24	2	40	0.337	15.1°N	Holasek et al., 1996; Kroll et al., 2021
Sarychev	3	6	0.1149	11–19	−0.150	48.1°N	Axebrink et al., 2025
Nabro	3	6	0.1188	9–14	0.485	13.4°N	Bourassa et al., 2012
Kelut	7	14	0.1186	25	0.676	7.9°S	Suzuki and Iguchi, 2019
Calbuco	5	11	0.1191	16–23	−0.673	41.3°S	Klekociuk et al., 2020
Raikoke	8	12	0.1199	12–13	0.029	48.3°N	Kloss et al., 2021
Hunga	6	14	6–8	58	0.651	20.5°S	Xu JY et al., 2022; Zhu YQ et al., 2022

Second, water vapor affects the aerosol lifetime in complex ways. Eruptions with low water vapor, such as Sarychev and Nabro, showed 6-month half lifetimes attributable to the low-altitude injection. Despite substantial water vapor, El Chichón and Pinatubo maintained 24-month half lifetimes, showing the dominant influence of the injection height. The Hunga eruption, characterized by a high SO_2 injection height (58 km), exhibited a 14-month aerosol half lifetime. Initially, the large water vapor caused rapid aerosol settling through radiative cooling. However, as the water vapor separated from the aerosol plume, the high injection altitude extended the aerosol half lifetime (Legras et al., 2022). Meanwhile, the rise in SWV could intensify the stratospheric Brewer–Dobson circulation (Li F and Newman, 2020), which facilitated a longer atmospheric residence of aerosol.

The vertical component W^* of the Brewer–Dobson circulation at 100 hPa is critical as well. When W^* exceeds 0.3 mm/s, it significantly extends the aerosol lifetime through enhanced vertical transport. This effect is evident in the Kelut eruption, where strong circulation compensated for lower injection height. Conversely, the 11-month half lifetime of Calbuco was influenced by a strong downward motion despite its greater injection height.

Latitude also affects the aerosol lifetime. The Pinatubo eruption at 15.1°N tended to have longer lifetimes because of weaker polar vortex interactions and its position in the ascending branch of the Brewer–Dobson circulation. Conversely, the Calbuco eruption at 41.3°S experienced a faster removal because of stronger polar circulation patterns.

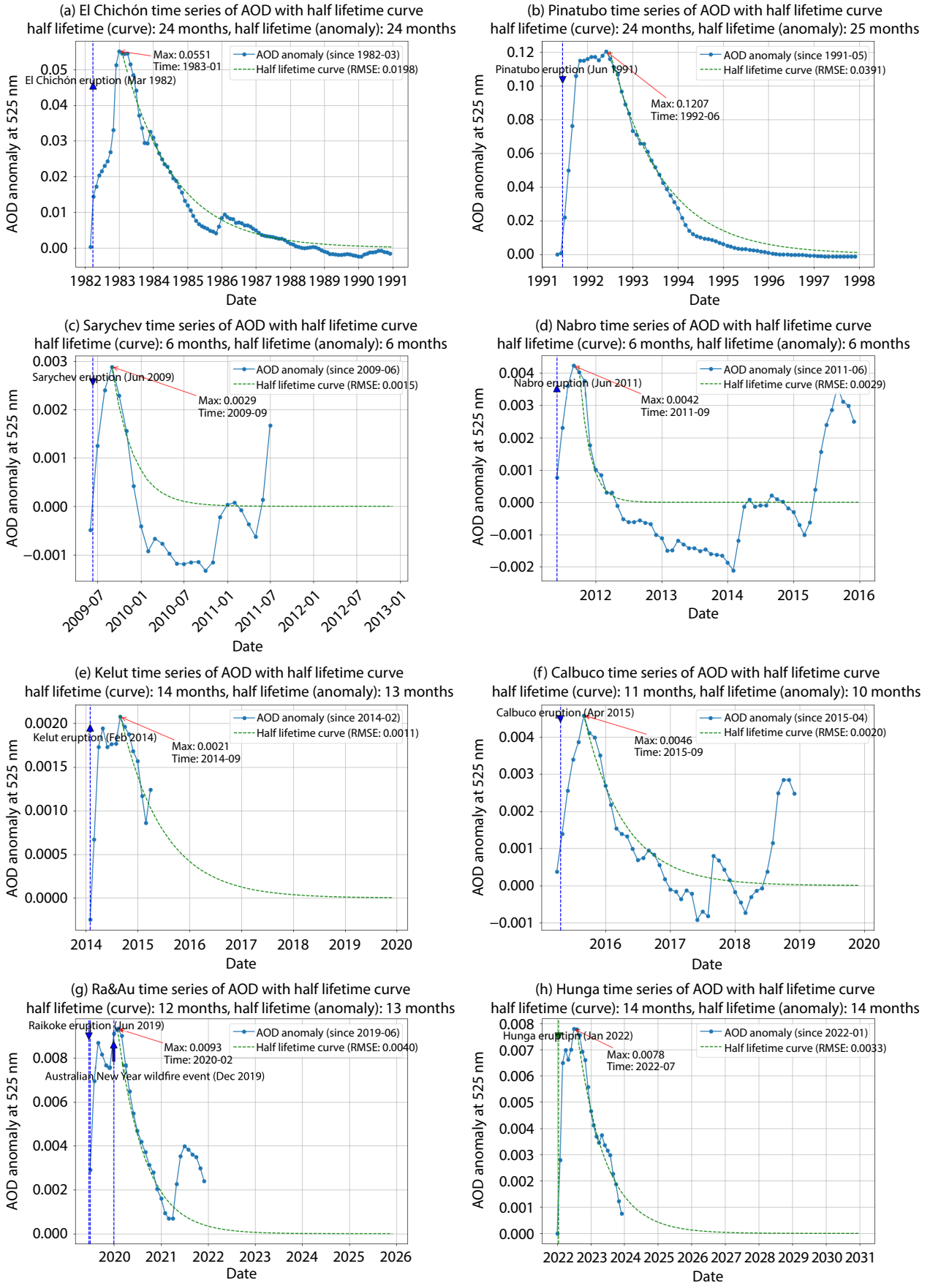

Figure 4. (a–h) Aerosol half lifetime fitting curves for each selected volcanic activity. Ra&Au, Raikoke eruption and Australian New Year wildfire event.

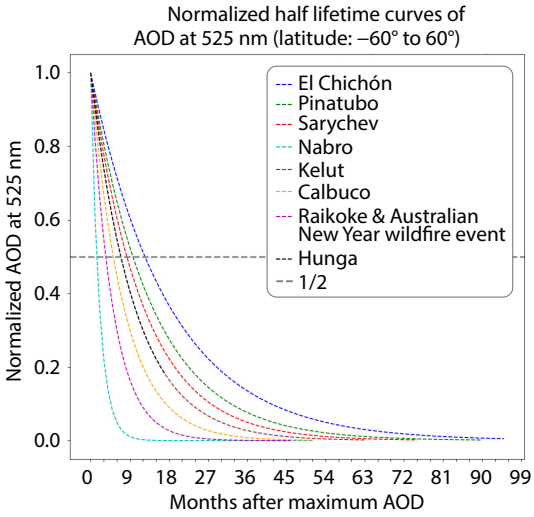

Figure 5. Normalized plot of the fitted curves for the half lifetimes of volcanic aerosols.

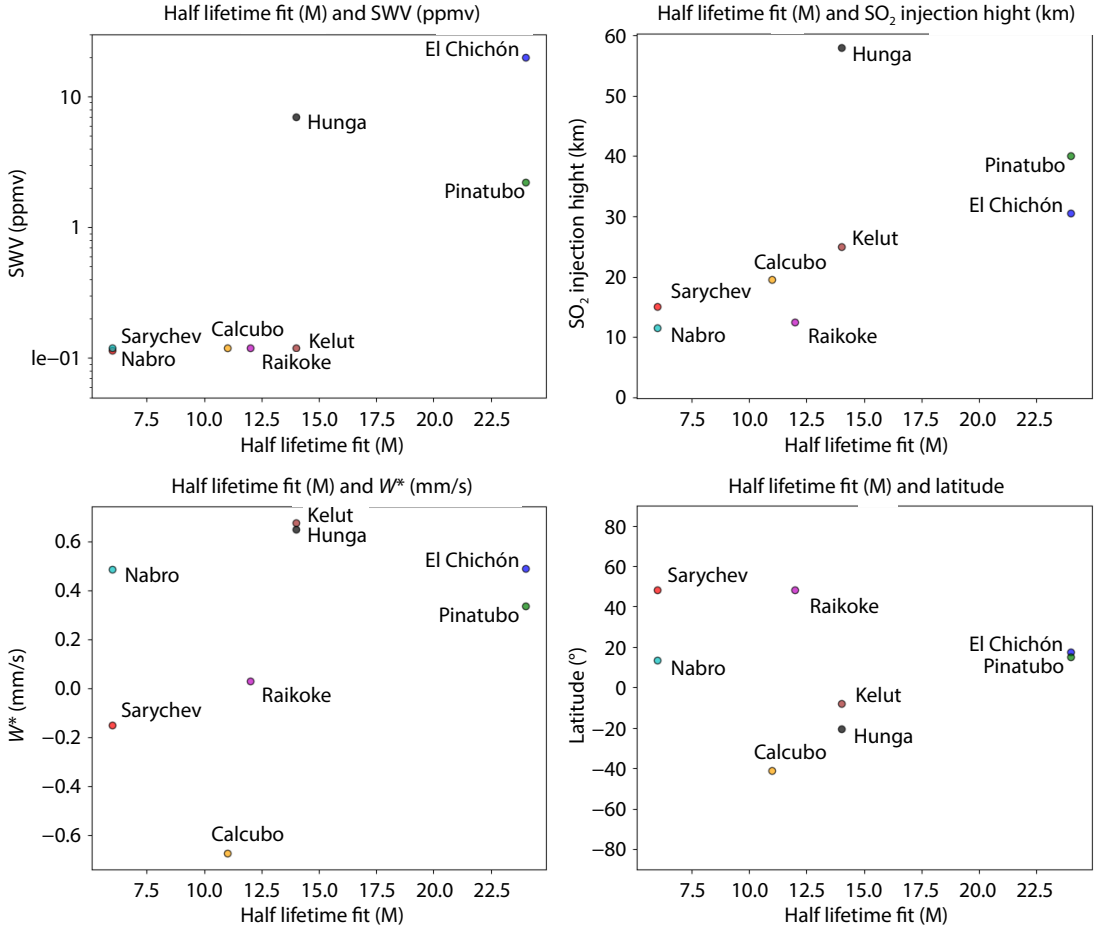

Figure 6. Scatterplots of aerosol half lifetimes fitted for each volcanic activity and the SWV, SO_2 injection height, vertical component W^* of the Brewer–Dobson circulation, and eruption latitude. M = months.

5. Conclusions

The Hunga eruption offered a unique opportunity to investigate the pivotal role of copious water vapor emissions in stratospheric aerosol plume dynamics. Initial observations indicated that both the water vapor and aerosol plumes exhibited latitudinal diffusion rates approximating 5° per month, but the timing of their arrival at the polar vortex differed. The aerosol plume lagged behind the water vapor plume for months, with the water vapor plume ascending to higher altitudes than the aerosol plume and spreading globally via the Brewer–Dobson circulation. The lifetime of the resulting sulfate aerosols was found to be modulated by competing factors: although the exceptionally high water vapor content

accelerated particle growth and gravitational settling, thereby shortening the aerosol half lifetime, this effect was partially counterbalanced by the extreme injection altitude, which bypassed tropospheric scavenging, and by the strength of the Brewer–Dobson circulation, which facilitated ascent and dispersion. The moderate half lifetime of 14 months observed for the Hunga aerosols reflects this complex interplay, where extreme water vapor loading still had a certain impact on the aerosol half lifetime. Furthermore, the comparative analysis highlighted how eruption-specific gas ratios shaped climate impacts. Unlike the Pinatubo eruption, the relatively low SO_2 emissions of Hunga relative to its immense water vapor resulted in limited AOD enhancements specifically in the northern high latitudes, underscoring the distinct climatic signature of submarine eruptions dominated by water vapor. Future investigations should prioritize the long-term radiative forcing implications of such unprecedented water vapor injections and their potential interactions with climate oscillations.

Acknowledgments

Xin Zhou acknowledges funding from the National Natural Science Foundation of China (Grant Nos. U2442210 and 42275059). Qing Zhao was supported by funding from Chengdu University of Information Technology (Grant No. X202310621039).

References

Axebrink, E., Sporre, M. K., and Friberg, J. (2025). Impact of SO_2 injection profiles on simulated volcanic forcing for the 2009 Sarychev eruptions—Investigating the importance of using high-vertical-resolution methods when compiling SO_2 data. *Atmos. Chem. Phys.*, *25*(4), 2047–2059. https://doi.org/10.5194/acp-25-2047-2025

Bourassa, A. E., Robock, A., Randel, W. J., Deshler, T., Rieger, L. A., Lloyd, N. D., Llewellyn, E. J., and Degenstein, D. A. (2012). Large volcanic aerosol load in the stratosphere linked to Asian monsoon transport. *Science*, *337*(6090), 78–81. https://doi.org/10.1126/science.1219371

Carey, S., and Sigurdsson, H. (1986). The 1982 eruptions of El Chichón volcano, Mexico (2): Observations and numerical modelling of tephra-fall distribution. *Bull. Volcanol.*, *48*(2-3), 127–141. https://doi.org/10.1007/BF01046547

Carr, J. L., Horváth, Á., Wu, D. L., and Friberg, M. D. (2022). Stereo plume height and motion retrievals for the record-setting Hunga Tonga-Hunga Ha'apai eruption of 15 January 2022. *Geophys. Res. Lett.*, *49*(9), e2022GL098131. https://doi.org/10.1029/2022GL098131

Evan, S., Brioude, J., Rosenlof, K. H., Gao, R. S., Portmann, R. W., Zhu, Y. Q., Volkamer, R., Lee, C. F., Metzger, J. M., … Read, W. G. (2023). Rapid ozone depletion after humidification of the stratosphere by the Hunga Tonga Eruption. *Science*, *382*(6668), eadg2551. https://doi.org/10.1126/science.adg2551

Fleming, E. L., Newman, P. A., Liang, Q., and Oman, L. D. (2024). Stratospheric temperature and ozone impacts of the Hunga Tonga-Hunga Ha'apai water vapor injection. *J. Geophys. Res.: Atmos.*, *129*(1), e2023JD039298. https://doi.org/10.1029/2023JD039298

Gupta, A. K., Mittal, T., Fauria, K. E., Bennartz, R., and Kok, J. F. (2025). The January 2022 Hunga eruption cooled the southern hemisphere in 2022 and 2023. *Communications Earth & Environment*, *6*(1), 240. https://doi.org/10.1038/s43247-025-02181-9

Hersbach, H., Bell, B., Berrisford, P., Biavati, G., Horányi, A., Muñoz Sabater, J., Nicolas, J., Peubey, C., Radu, R., … Thépaut, J. N. (2020). The ERA5 global reanalysis. *Q J R Meteorol Soc.*, *146*(730), 1999–2049. https://doi.org/10.1002/qj.3803

Holasek, R. E., Self, S., and Woods, A. W. (1996). Satellite observations and interpretation of the 1991 Mount Pinatubo eruption plumes. *J. Geophys. Res.: Solid Earth*, *101*(B12), 27635–27655. https://doi.org/10.1029/96JB01179

Jenkins, S., Smith, C., Allen, M., and Grainger, R. (2023). Tonga eruption increases chance of temporary surface temperature anomaly above 1.5°C. *Nat. Clim. Chang.*, *13*(2), 127–129. https://doi.org/10.1038/s41558-022-01568-2

Khaykin, S., Podglajen, A., Ploeger, F., Grooß, J. U., Tence, F., Bekki, S., Khlopenkov, K., Bedka, K., Rieger, L., … Ravetta, F. (2022). Global perturbation of stratospheric water and aerosol burden by Hunga eruption. *Commun. Earth Environ.*, *3*, 316. https://doi.org/10.1038/s43247-022-00652-x

Klekociuk, A. R., Ottaway, D. J., MacKinnon, A. D., Reid, I. M., Twigger, L. V., and Alexander, S. P. (2020). Australian Lidar measurements of aerosol layers associated with the 2015 Calbuco eruption. *Atmosphere*, *11*(2), 124. https://doi.org/10.3390/atmos11020124

Kloss, C., Berthet, G., Sellitto, P., Ploeger, F., Taha, G., Tidiga, M., Eremenko, M., Bossolasco, A., Jégou, F., … Legras, B. (2021). Stratospheric aerosol layer perturbation caused by the 2019 Raikoke and Ulawun eruptions and their radiative forcing. *Atmos. Chem. Phys.*, *21*(1), 535–560. https://doi.org/10.5194/acp-21-535-2021

Kroll, C. A., Dacie, S., Azoulay, A., Schmidt, H., and Timmreck, C. (2021). The impact of volcanic eruptions of different magnitude on stratospheric water vapor in the tropics. *Atmos. Chem. Phys.*, *21*(8), 6565–6591. https://doi.org/10.5194/acp-21-6565-2021

Legras, B., Duchamp, C., Sellitto, P., Podglajen, A., Carboni, E., Siddans, R., Grooß, J. U., Khaykin, S., and Ploeger, F. (2022). The evolution and dynamics of the Hunga Tonga–Hunga Ha'apai sulfate aerosol plume in the stratosphere. *Atmos. Chem. Phys.*, *22*(22), 14957–14970. https://doi.org/10.5194/acp-22-14957-2022

Li, F., and Newman, P. (2020). Stratospheric water vapor feedback and its climate impacts in the coupled atmosphere–ocean Goddard Earth Observing System Chemistry-Climate Model. *Climate Dyn.*, *55*(5), 1585–1595. https://doi.org/10.1007/s00382-020-05348-6

Manney, G. L., Santee, M. L., Lambert, A., Millán, L. F., MI Schwaner, K., Werner, F., Lawrence, Z. D., Read, W. G., Livesey, N. J., and Wang, T. (2023). Siege in the southern stratosphere: Hunga Tonga–Hunga Ha'apai water vapor excluded from the 2022 Antarctic polar vortex. *Geophys. Res. Lett.*, *50*(14), e2023GL103855. https://doi.org/10.1029/2023GL103855

Millán, L., Santee, M. L., Lambert, A., Livesey, N. J., Werner, F., Schwartz, M. J., Pumphrey, H. C., Manney, G. L., Wang, Y., … Froidevaux, L. (2022). The Hunga Tonga-Hunga Ha'apai hydration of the stratosphere. *Geophys. Res. Lett.*, *49*(13), e2022GL099381. https://doi.org/10.1029/2022GL099381

NASA/LARC/SD/ASDC. (2024). Global Space-based Stratospheric Aerosol Climatology Version 2.22 [Dataset]. Hampton, Virginia, USA: NASA Langley Atmospheric Science Data Center DAAC. https://doi.org/10.5067/GLOSSAC-L3-V2.22

Proud, S. R., Prata, A. T., and Schmauß, S. (2022). The January 2022 eruption of Hunga Tonga-Hunga Ha'apai volcano reached the mesosphere. *Science*, *378*(6619), 554–557. https://doi.org/10.1126/science.abo4076

Schoeberl, M. R., Wang, Y., Ueyama, R., Taha, G., Jensen, E., and Yu, W. (2022). Analysis and impact of the Hunga Tonga-Hunga Ha'apai stratospheric water vapor plume. *Geophys. Res. Lett.*, *49*(20), e2022GL100248. https://doi.org/10.1029/2022GL100248

Schoeberl, M. R., Toohey, M., Wang, Y., and Ueyama, R. (2025). Stratospheric injection lifetimes. *J. Geophys. Res.-Atmos.*, *130*(18), e2025JD043928. https://doi.org/10.1029/2025JD043928

Sellitto, P., Podglajen, A., Belhadji, R., Boichu, M., Carboni, E., Cuesta, J., Duchamp, C., Kloss, C., Siddans, R., … Legras, B. (2022). The unexpected radiative impact of the Hunga Tonga eruption of 15th January 2022. *Commun. Earth Environ.*, *3*, 288. https://doi.org/10.1038/s43247-022-00618-z

Stenchikov, G., Ukhov, A., and Osipov, S. (2025). Modeling the radiative forcing and atmospheric temperature perturbations caused by the 2022 Hunga volcano explosion. *J. Geophys. Res.-Atmos.*, *130*, e2024JD041940. https://doi.org/10.1029/2024JD041940

Suzuki, Y. J., and Iguchi, M. (2019). Determination of the mass eruption rate for the 2014 Mount Kelud eruption using three-dimensional numerical simulations of volcanic plumes. *J. Volcanol. Geoth. Res.*, *382*, 42–49. https://doi.org/10.1016/j.jvolgeores.2017.06.011

Taha, G., Loughman, R., Zhu, T., Thomason, L., Kar, J., Rieger, L., and Bourassa, A. (2021). OMPS LP Version 2.0 multi-wavelength aerosol extinction coefficient retrieval algorithm. *Atmos. Meas. Tech.*, *14*, 1015–1036. https://doi.org/10.5194/amt-14-1015-2021,2021

Taha, G., Loughman, R., Colarco, P. R., Zhu, T., Thomason, L. W., and Jaross, G. (2022). Tracking the 2022 Hunga Tonga-Hunga Ha'apai aerosol cloud in the upper and middle stratosphere using space-based observations. *Geophys. Res. Lett.*, *49*(19), e2022GL100091. https://doi.org/10.1029/2022GL100091

Toohey, M., Jia, Y., Khanal, S., and Tegtmeier, S. (2025). Stratospheric residence time and the lifetime of volcanic stratospheric aerosols. *Atmos. Chem. Phys.*, *25*(6), 3821–3839. https://doi.org/10.5194/acp-25-3821-2025

Walter, L. S., and de Silva, S. (1991). Volcanism–Climate Interactions. *NASA Conference Publication 10062*, Goddard Space Flight Center.

Waters, J. W., Froidevaux, L., Harwood, R. S., Jarnot, R. F., Pickett, H. M., Read, W. G., Siegel, P. H., Cofield, R. E., Filipiak, M. J., … Walch, M. J. (2006). The Earth observing system microwave limb sounder (EOS MLS) on the aura Satellite. *IEEE Trans. on Geoscience and Remote Sensing*, *44*(5), 1075–1092. https://doi.org/10.1109/TGRS.2006.873771

Xu, J. Y., Li, D., Bai, Z. X., Tao, M. C., and Bian, J. C. (2022). Large amounts of water vapor were injected into the stratosphere by the Hunga Tonga–Hunga Ha'apai volcano eruption. *Atmosphere*, *13*(6), 912. https://doi.org/10.3390/atmos13060912

Zhou, X., Dhomse, S. S., Feng, W. H., Mann, G., Heddell, S., Pumphrey, H., Kerridge, B. J., Latter, B., Siddans, R., … Chipperfield, M. P. (2024). Antarctic vortex dehydration in 2023 as a substantial removal pathway for Hunga Tonga-Hunga Ha'apai water vapor. *Geophys. Res. Lett.*, *51*(8), e2023GL107630. https://doi.org/10.1029/2023GL107630

Zhu, Y. Q., Bardeen, C. G., Tilmes, S., Mills, M. J., Wang, X. Y., Harvey, V. L., Taha, G., Kinnison, D., Portmann, R. W., … Toon, O. B. (2022). Perturbations in stratospheric aerosol evolution due to the water-rich plume of the 2022 Hunga-Tonga eruption. *Commun. Earth Environ.*, *3*, 248. https://doi.org/10.1038/s43247-022-00580-w